



GEOQuébec
2015

Challenges from North to South
Des défis du Nord au Sud

Lateral Performance of Helical Tapered Piles in Sand

Ahmed Fahmy, Mohamed Hesham El Naggar
Department of Civil and Environmental Engineering
The University of Western Ontario, London, Ontario, Canada

ABSTRACT

A novel piling system is proposed in this study to support solar energy panels in solar farm projects. It involves a spun-cast ductile iron (SCDI) tapered pile fitted with a lower helix. The proposed pile offers higher lateral capacity, and represents a sustainable foundation system. The monotonic lateral performance of the proposed system is investigated herein. Five SCDI tapered and two steel straight shaft piles were installed using mechanical torque in silty sand. The piles were laterally tested and their ultimate capacities were evaluated. The effect of prior axial and cyclic lateral loading on the piles' lateral performance was assessed. The tapered piles generally possess a stiffer response and higher ultimate capacity. The fixation provided by the helix had a positive effect on the lateral performance of short piles.

RÉSUMÉ

Un système novateur de pieux, visant à supporter les panneaux solaires pour un projet de ferme solaire est présenté dans cette étude. Il s'agit de pieux coniques en fonte centrifugée munis d'une hélice inférieure. Ce type de pieu offre une capacité portante latérale supérieure, ainsi qu'un système plus durable de fondation. La performance latérale sous charge monotone pour ce type de pieu est détaillée dans cet article. Cinq pieux coniques en fonte centrifugée, ainsi que deux pieux en acier à tige droite ont été installés par un couple mécanique dans un sable silteux. Pour chacun, un chargement transversal a été appliqué afin de déterminer leur capacité maximale. L'effet, sur la performance latérale, des chargements axiaux et des chargements cycliques latéraux, a été évalué. Les pieux coniques présentent un comportement plus rigide, ainsi qu'une plus grande capacité portante maximale. La fixation offerte par la présence de l'hélice sur le pieu, entraîne un effet positif sur la performance latérale des pieux de petites longueurs.

1 INTRODUCTION

While almost all pile foundations are subjected to some lateral loading (Fleming, *et al.*, 2009), it could be considerably large in cases such as offshore structures, transmission towers and high rise buildings. Tapered piles have been successfully used for many years as an efficient piling system to support axial loads capacity (El Naggar & Wei, 1999). In their experimental investigation, El Naggar and Wei (1999) reported that tapered piles installed in cohesionless soils exhibited stiffer response than cylindrical piles at various load levels with more pronounced effects at low confining pressures. They also reported an increase in lateral capacity as high as 77% for a pile taper angle as small as 0.95° .

Owing to their geometry, tapered piles provide an efficient material distribution and have greater flexural rigidity at their top portion, and hence increased lateral stiffness. Sakr *et al.* (2005) investigated the lateral performance of FRP composite tapered piles installed using a toe-driving technique. The composite tapered piles exhibited stiffer response and larger lateral resistance compared to conventional piles. Considering the ultimate load criteria suggested by (Prakash & Sharma, 1990), the lateral capacity of tapered piles was found to reach up to 200% of the capacity of a cylindrical pile of the same average diameter (Sakr *et al.*, 2005).

Helical piles are gaining wide popularity fuelled by recent advances in construction equipment, which allow further development of these piles, and facilitate their application in projects that subject them to unique and complex loading conditions. Different helical pile systems with large diameter shafts were developed recently offering large lateral capacities (Elkasabgy, 2011; Fleming *et al.*, 2009).

Helical piles are easy to install with low levels of noise and vibration. However, their installation can cause disturbance of the adjacent soil within the zone affected by the penetration of the pile shaft and helices, thus reducing the soil shear strength and consequently, the pile shaft capacity (axial and lateral) is significantly reduced (Bagheri & El Naggar, 2013). The lateral load resistance of long helical piles can be generally estimated using the same techniques adopted for cylindrical piles; however, the installation effects need to be considered in choosing suitable design soil parameters (Puri *et al.*, 1984).

The presence of helical plates at shallow depth can increase the pile's lateral capacity. Prasad and Rao (1996) experimentally studied the lateral response of helical piles in clay. They found that their lateral capacity is generally equal to 1.2 to 1.5 times that of a straight shaft with no helical plates. In addition to the shaft resistance, the developed bearing/uplift resistance on the front/back half of the helical plates once rotated and the friction on the plates' surfaces contribute to the lateral resistance (Prasad & Rao, 1996). For helical piles with helices placed at greater depths, however, the lateral performance is mainly controlled by the pile shaft (Puri *et al.*, 1984).

2 OBJECTIVES AND SCOPE OF WORK

This article examines the lateral behavior of an innovative pile that combines the efficiency of the tapered section and the construction advantage of helical piles. The proposed piling system consists of a spun-cast ductile iron tapered pile (Seamless-Pole-Inc., 2010) fitted with a lower helical plate to facilitate its installation. The

pile is to be installed using a mechanical torque delivered by a driving motor holding the pile head.

In order to assess the feasibility and efficiency of the proposed system, 16 field load tests were performed to evaluate its lateral performance under monotonic conditions. The effects of the prior cyclic tests on the system monotonic performance was also evaluated

3 EXPERIMENTAL SETUP

3.1 Soil investigation

One borehole was drilled in the vicinity of the test piles at the location shown in Figure 1. The borehole log shows that the soil profile comprises silty sand/gravelly sand layers that extend from the ground surface to 9.00m below ground surface, followed by a hard silty till that extends to the end of the borehole (i.e. 11m depth). The ground water table was found at 3.5m from the ground surface.

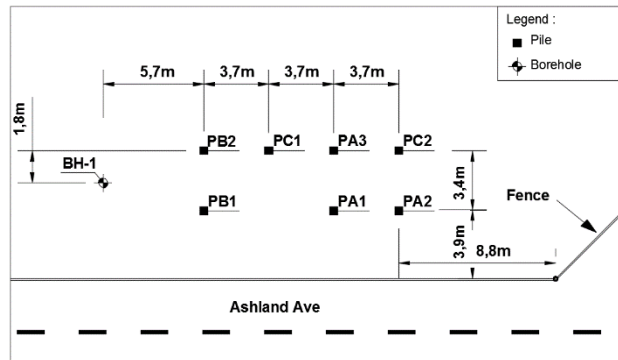


Figure 1: Site layout showing the drilled borehole location

3.1.1 Field tests

A Standard Penetration Test (SPT) was conducted with blow count measurements taken at 0.75m intervals. These values were corrected for hammer energy efficiency and other field procedure conditions to obtain N_{60} , i.e. (Skempton, 1986)

$$N_{60} = \frac{N C_R C_S C_B E_m}{0.6} \quad [1]$$

where:

C_S is sampler correction, equal to 1.2 where sampler without liner was used

C_R is drill rod length correction, equal to 0.75

C_B is borehole diameter correction, equal 1.15 for diameter $D=200\text{mm}$

E_m is hammer efficiency, equal to 0.8 for hammer used (Bowles, 1996)

These values were then corrected for the overburden pressure producing N_{60}' , i.e., (Liao & Whitman, 1986)

$$N_{60}' = N_{60} \sqrt{\frac{100}{\sigma_v'}} \quad [2]$$

Where σ_v' is the effective overburden stresses.

The resulting variation of N_{60}' with depth along the top 4m of main interest in this study is presented in Figure 2 (b).

The sand-cone test (ASTM D1556, 2007) was employed to measure the soil in-situ unit weight. The top 0.5m of soil was excavated, and two sand-cone tests were performed on the underlying layer. The average measured bulk density was 16.5kN/m^3 .

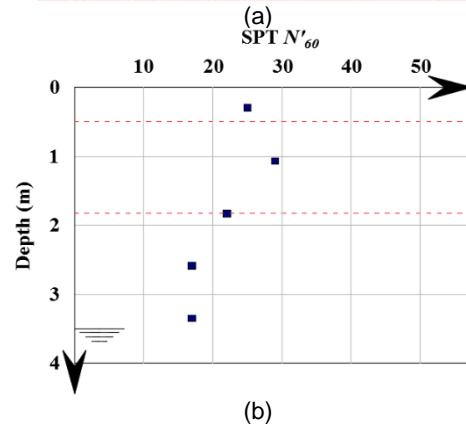


Figure 2: (a) General soil stratification; (b) Variation of SPT N'_{60} with depth

3.1.2 Laboratory testing

Fifteen disturbed samples retrieved from the SPT split-spoon sampler were transported and subjected to various laboratory tests. The tests included soil classification, determination of the specific gravity, G_s , measurement of water content, W_c , direct shear tests and Atterberg limit determination.

Soil classification and index properties

Sieve analyses of the extracted samples at different depths were performed according to ASTM C136 (2014).

The tested piles were only 3.1m long, with an even shorter effective embedment depth due to their free length. Thus, only the top 4m of soil affect the pile response to lateral loads. The soil sample at 1.05m depth was deemed representative of soil properties along the pile shaft. The resulting classification curve presented in Figure 3 showed that the soil within that depth has only 14.8% fines and almost 0% Gravel. Atterberg limits of three samples were measured showing average liquid and plastic limits of 25.3% and 21.5%, respectively (ASTM D4318, 2010). The top layer is thus classified as silty sand (SM) according to the Unified Soil Classification

System USCS (ASTM D2487, 2011). Lower percentages of fines were found at deeper layers and higher percentages at the bottom of the borehole. The average measured G_s of two soil samples extracted at depths of 1.05m and 4.8m was found to be 2.71. The average in-situ W_c was measured to be 20.5%.

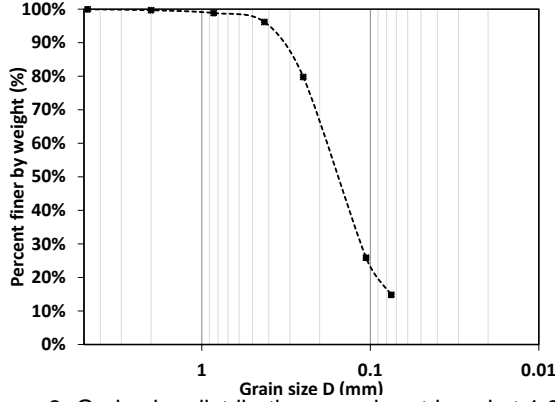
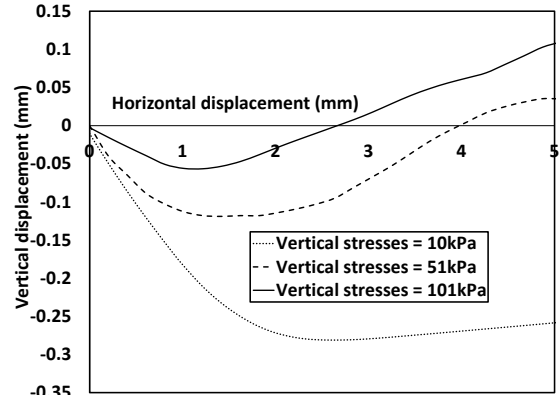
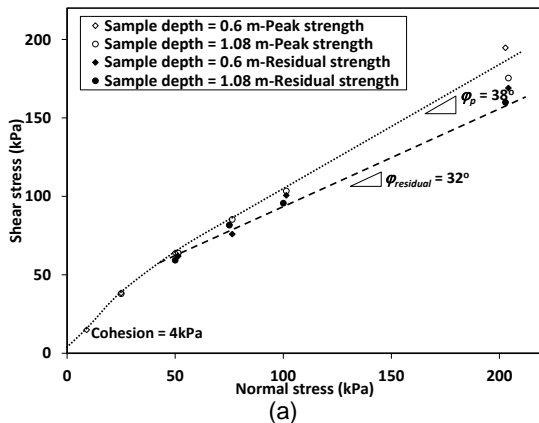


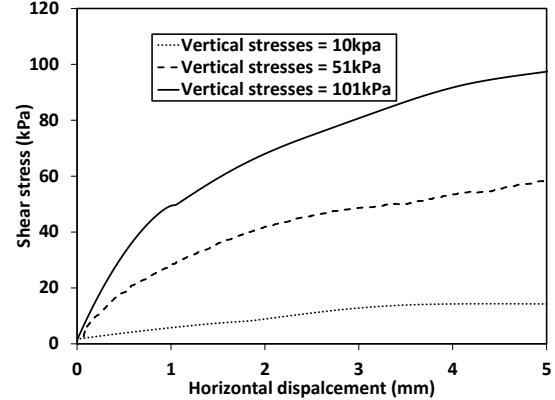
Figure 3: Grain size distribution-sample retrieved at 1.05m below ground surface

Soil shear strength parameters

Direct shear tests (ASTM D3080, 2011) were conducted on soil specimens retrieved at 0.6m and 1.08m depths in order to determine their shear strength parameters. The horizontal rate of feed was 0.406mm/min. The unit weight of the tested specimens within the direct shear box was set to the field measured value. The variation of shear stresses with normal stresses, vertical displacement and horizontal displacement as well as the residual and peak strength values are presented in Figure 4. A bilinear shear-normal stress relation was observed with the first section ending at a normal stress of 20kPa. Based on the direct shear test results, the effective cohesion, c' , residual angle of internal friction $\phi_{residual}$ and peak angle of internal friction ϕ_p were determined to be 4 kPa, 32° and 38° , respectively. The determined angle of internal friction lies within the upper bound of the relevant range typically found in the literature for the range of SPT N values at the location of test specimen, due to the high angularity of the sand particles (Bowles, 1996).



(b)



(c)

Figure 4: Direct shear tests results (a) Shear vs normal stresses; (b) Vertical displacement vs horizontal displacement; (c) Shear stress vs horizontal displacement

Relative density and stiffness parameters

The soil relative density D_r , Young's modulus E_s , and Poisson's ratio ν were correlated to the corrected N_{60} values. For example, D_r was correlated to the corrected N'_{60} , i.e. (Mayne *et al.*, 2002):

$$D_r = 100 \sqrt{\frac{N'_{60}}{60}} \quad [3]$$

The variation of D_r along the top 4m ranges between 50 to 70%, hence, the soil deposits along the pile length can be classified as medium dense to dense sand (Bowles, 1996).

In absence of undisturbed soil samples, the over-consolidation ratio, OCR, is generally correlated to other parameters or test results. The apparent preconsolidation pressure σ_p' for the Sand was correlated to N_{60} , i.e., (Mayne, 1992):

$$\sigma_p' = 0.47 (N_{60})^m P_a \quad [4]$$

where P_a is the atmospheric pressure, $m = 0.6$ to 0.8 for silty sands/sandy silts (Mayne, 2006).

The variation of σ_p' with depth was obtained employing Eq. 4 and knowing the initial overburden stresses, the OCR was calculated to be approximately 6 for the top 4

m. This is attributed to the fact that the site is used for storage of heavy steel tanks.

Although several correlations have been developed for soil elastic modulus, E_s , and the measured SPT N , a significant scatter exists between the different correlations. For overconsolidated sand, E_s can be correlated to the corrected SPT N_{60} , i.e. (Kulhawy & Mayne, 1990):

$$E_s/P_a = 15N_{60} \quad [5]$$

It should be noted, however, that the post-installation values are of main interest to this study. For that, and as a preliminary estimation, the recommended values by Poulos & Davis (1980) for driven piles in sand were considered. They suggested that, while E_s for sand typically varies with depth, it is appropriate for analysis purposes to consider an average modulus value along the pile shaft and greater values below the toe of driven piles (Poulos & Davis, 1980). This is also acceptable considering the relatively short length of the piles in the present study. Average values suggested by Poulos & Davis were in the order of 55–70MPa for medium dense sand and 70–100MPa for dense sand layers. Accordingly, an average E_s of 70MPa was considered for the current soil profile.

The value of ν ranges between 0.2 to 0.4 for loose to dense Sands (AASHTO, 2002) hence 0.3 will be considered.

Finally, considering the average OCR of 6 along the first 4m, the average coefficient of earth pressure at rest prior to the pile installation can be given by (Mayne & Kulhawy, 1982):

$$K_o-OCR = (1-\sin\phi)OCR \quad (1-\sin\phi) = 0.76 \quad [6]$$

It should be noted that the soil properties obtained from the laboratory tests represented the soil state prior to the piles installation therefore neglecting the effects of pile installation torque, the top soil predrilling prior to the piles installation as well as the axial load tests performed before the lateral ones. The representative soil parameters are summarized in Table 1.

Table 1: Representative soil parameters

| Depth (m) | | $\phi_p(\theta)$ | c' (kPa) | G_s | W_c (%) | ν | E_s (MPa) | γ (kN/m ³) |
|-----------|-----|------------------|------------|-------|-----------|-------|-------------|-------------------------------|
| From | To | | | | | | | |
| 0 | 0.5 | 36 | 4 | 2.71 | 20.5 | 0.3 | 70 | 16.5 |
| 0.5 | 4 | 38 | | | | | | |

3.2 Test Piles

Seven hollow closed-end piles with configurations as shown in Figure 5 were installed using torque. Three piles were of configuration A, two of configuration B and two of configuration C. The piles of configurations A and B were made of ductile iron with rough surface as shown in Figure 6. Configuration C piles were made of straight shaft steel pipe, which was considered for comparison purposes. The wall thickness of all piles was 5.5mm.

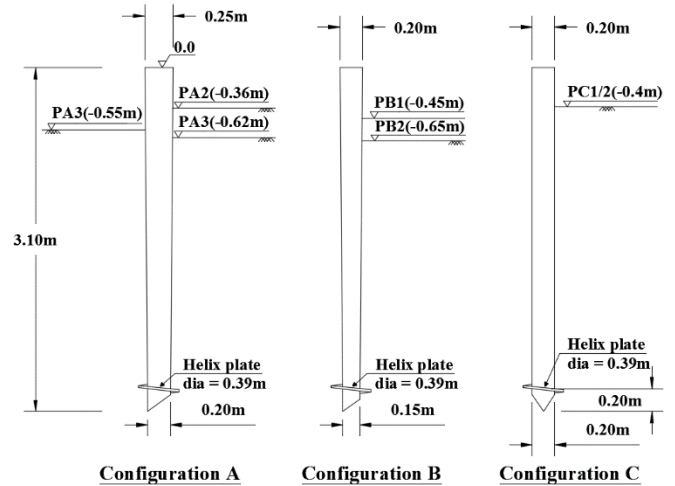


Figure 5: Tested piles configurations



Figure 6: Image of the piles external surface – configurations A and B (Seamless-Pole-Inc., 2010)

3.3 Instrumentation and Test Setup

A special setup was designed and fabricated to apply the lateral loading to the piles, which involved loading two piles against each other as shown in Figure 7. In this setup, the load was transferred to the piles through steel clamps connected to a main loading rod by a hinged connection ensuring a free head condition. Clamps with different diameters were manufactured to fit the different test piles configurations. The applied load was measured using a load cell incorporated into the loading setup as demonstrated in Figure 7.

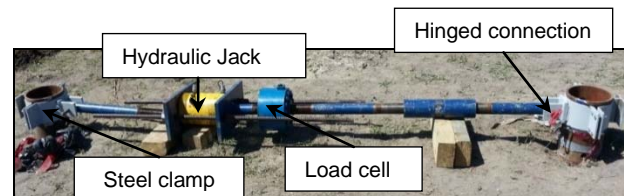


Figure 7: Image of Lateral loading setup

In order to measure the pile head displacement, two linear variable displacement transducers (LVDTs) were supported on an independent beam and their measuring tips were pushing against a steel plate attached to the pile head as shown in Figure 8. The LVDTs and load cell were connected to a data acquisition system, which recorded the readings every 1 second.



Figure 8: Lateral load setup: steel clamp/LVDT plate

3.4 Installation Procedure

The torque employed to install the piles was delivered using a Hitachi UH07 rig, and was applied through a specially manufactured steel cap bolted to the pile head as shown in Figure 9. The cap was then removed before the start of the lateral testing.

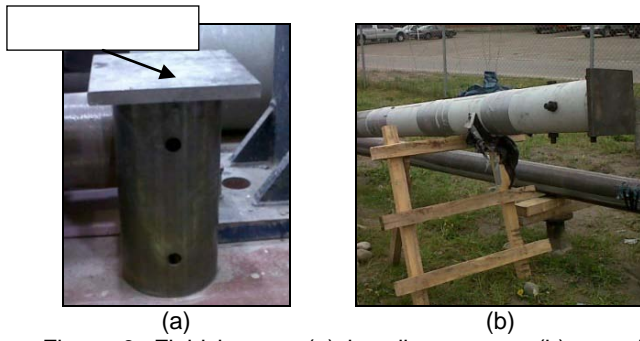


Figure 9: Field images (a) installatopn cap, (b) cap-pile connection

Following installation, the inclination angle of the pile head with the vertical axis was measured to examine the piles verticality. The maximum inclination angle measured was less than 2° . The piles free (unsupported) lengths at the start of lateral loading are shown in Figure 5.

3.5 Load Test Sequence and Test Procedure

The lateral load tests were conducted on pairs of piles. The sequence of load tests is presented in Table 2. It should be noted that prior to the lateral load tests, piles PA1, PA2, PB1 and PC1 were prior tested in cyclic compression whereas PA3, PB2 and PC2 were tested in monotonic uplift.

Table 2: Lateral pile test setups

| Test setup # | 1st pile | 2nd pile | Notes |
|--------------|----------|----------|-----------------------------|
| 1 | PA1 | PA2 | |
| 2 | PA3 | PC1 | |
| 3 | PB1 | PB2 | |
| 4 | PA3 | PC2 | PA3 prior tested in setup#2 |

The piles were loaded monotonically first, followed by two-way cyclic load test. The piles were then loaded monotonically again to evaluate the effect of cyclic loading on their lateral capacity. The pile load testing patterns are illustrated in Figure 10.

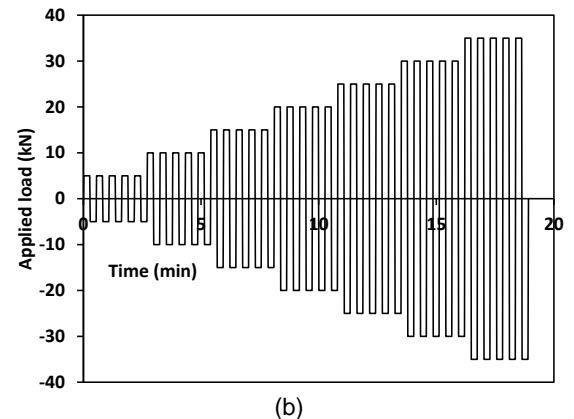
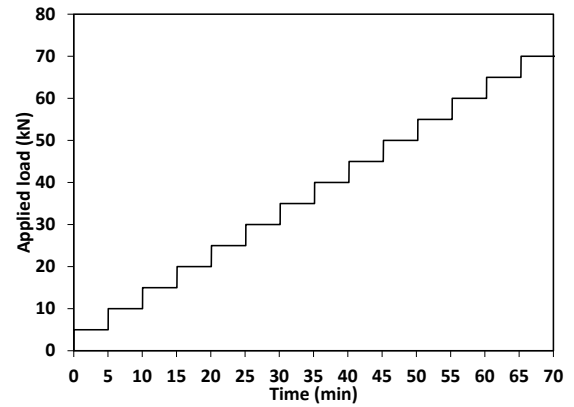


Figure 10: Lateral pile loading test patterns (a) Monotonic tests; (b) Cyclic tests

4 RESULTS AND DISCUSSION

4.1 Load-deflection curves

The measured load-deflection curves for the piles are presented in Figure 11 and Figure 12. Generally, all piles exhibited a stiff behavior with minor non-linear plastic zone and no clear global failure/plastic zone until the termination of the test. This behavior is attributed to the high flexural rigidity of the pile, the rough pile surface and the helix passive resistance.

Figure 11 presents the results for initial monotonic load tests (before lateral cyclic loading). It is noted that the load-deflection curves are hyperbolic in shape but no sign of failure up to the end of the tests. The performance of the tapered piles of configuration A was better than the piles of configurations B and C in terms of stiffer behavior and higher capacity. The only exception is setup#4 where PA3 showed softer behavior than PC2 because PA3 was tested first in setup#2, which might have resulted in soil failure and hence its strength was characterized by residual strength rather than the peak strength. It can also be noted from Figure 11 that, in general, tapered piles performed better than straight shafts, especially at higher lateral load levels. At lower load levels, the behavior is believed to be governed by the fixation provided by the helix plate whereas at greater level of loads the pile diameter/stiffness governs the behavior.

Piles of configuration B exhibited softer response than configuration C because they were subjected to uplift loading prior to lateral loading, and the piles were lifted up for more than 20cm hence releasing the initial lateral confinement of the pile surrounding soil and reducing its lateral resistance and increasing the unsupported length of the pile at the start of the lateral test as shown in Figure 5. In addition, the helical plates of piles configuration B were cracked/broken during the uplift loading as observed upon retrieving the piles after test completion.

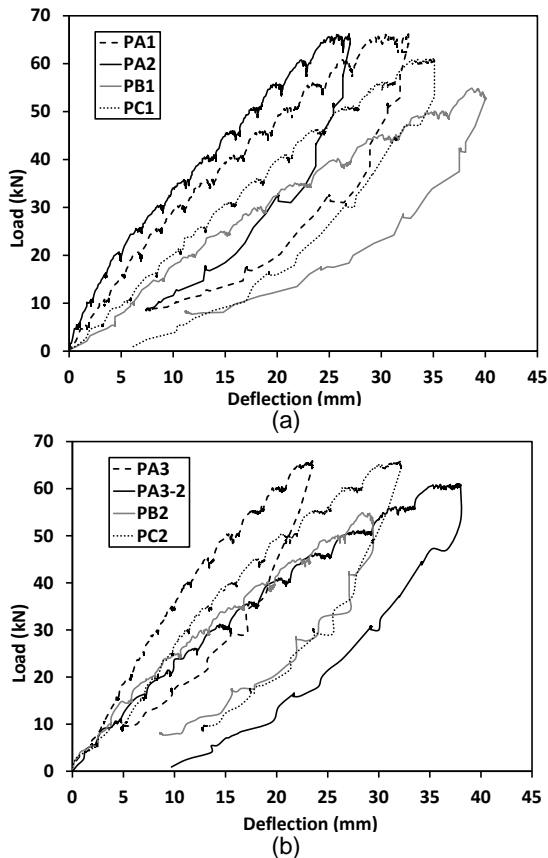


Figure 11: Load-deflection curves before cyclic lateral load tests: (a) Piles tested in axial compression before lateral loading; (b) Piles tested in uplift before lateral loading

Figure 12 presents the load-deflection curves for monotonic load tests conducted after the cyclic lateral load tests. The curves exhibit an initial lower stiffness segment due to the loosening of the sand in the vicinity of the pile, and even gap opening, during the cyclic loading. The stiffness reduction (softening) due to gapping was also reported by Pender and Pranjoto (1996) for piles subjected to cyclic lateral loading. An image of the gap formed behind pile PC1 is shown Figure 13. As the load progressed, the loose caved-in sand was re-compressed/gap closed and the stiffness increased again (i.e. strain hardening) as discussed by Allotey and El Naggar (2008). As the load continued to increase, the soil displayed nonlinear behavior and the pile stiffness started to decrease again.

While initially configuration C piles showed softer behavior than configuration A piles as shown in Figure 11, the higher degradation effect during the cyclic loading of the latter configuration compared to configuration C piles resulted in the opposite behavior when tested following the cyclic tests as shown in Figure 12.

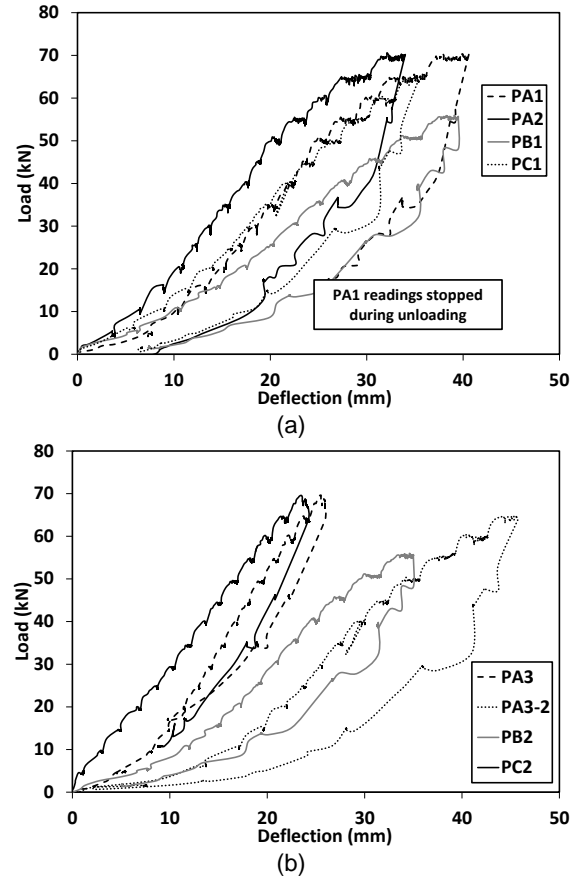


Figure 12: Load-deflection curves after cyclic lateral load tests: (a) Piles tested in axial compression before lateral loading; (b) Piles tested in uplift before lateral loading



Figure 13: An image of the developed gap behind pile PC1 at the end of the cyclic lateral testing

4.2 Pile Ultimate Capacity

While the piles lateral capacity depends on the supported structure deformation tolerance, two criteria are generally adopted to define the ultimate pile lateral capacity; the first defines the ultimate load as the load corresponding to the

intersection of the tangents to the load–deflection curve, while the second defines the failure load as the load corresponding to a specific deflection value (typically either 6.25 mm or 12.5 mm) (Prakash & Sharma, 1990). The first criterion was not considered since no clear plastic deformation and failure zones were observed in the load deflection curves (inability to draw the second tangent). Hence, the second criterion was employed herein, and the loads corresponding to 6.25 mm and 12.5 mm are noted. Unfortunately, the loading bar was touching the ground during the lateral load test of PC2 after cyclic loading, which rendered its results unreliable. The resulting values of ultimate pile capacity are summarized in Table 3.

In general, tapered piles of configuration A provided the highest capacity. However, because of the difference in average pile diameter and embedded pile length, it is more appropriate to present the results in terms of the pile capacity per unit volume. These values are obtained by normalizing the capacity of the piles presented in Table 3 by their embedded volume, and the results are presented in Table 4.

Inspecting the results in Table 4, it is clear that the tapered piles (configurations A and B) provided higher capacity per unit volume in comparison with the straight shaft piles for the case of initial lateral monotonic loading. The increase in capacity per unit volume was up to 82% for configuration A over configuration C piles. The result of the load tests after cyclic loading showed that all piles exhibited significant decrease in their capacity. However, the reduction in capacity was larger for the case of tapered piles. This was attributed to the larger degradation in soil stiffness and strength near the surface for the case of tapered piles because their free length was larger, which resulted in larger moment in addition to the lateral loading effects.

Upon unloading, the piles recovered 61% to 85% of their maximum displacement which implies significant plastic strains due to the rearrangement of the soil particles as well as the possible crushing of the sand particles.

Table 3: Ultimate lateral static capacity

| Pile# | Lateral capacity (kN) | | | |
|-------|-----------------------|-------------------|-------------------|-------------------|
| | Before cyclic test | | After cyclic test | |
| | 2.5mm deflection | 6.25mm deflection | 12.5mm deflection | 6.25mm deflection |
| PA1 | 20.2 | 34.3 | 4.8 | 16.3 |
| PA2 | 24.5 | 39.4 | 10.4 | 27.3 |
| PA3 | 23.2 | 43.4 | 6.6 | 24.4 |
| PB1 | 10.3 | 21.3 | 5.7 | 14.4 |
| PB2 | 18 | 29.4 | 4.6 | 12.2 |
| PC1 | 13 | 25.7 | 7.9 | 18.9 |
| PC2 | 14 | 34.5 | N/A | N/A |

Table 4: Ultimate static capacity per unit embedded volume of the tested piles

| Pile# | Capacity per unit volume (MN/m ³) | | | |
|-------|---|-------------------|-------------------|-------------------|
| | Before cyclic test | | After cyclic test | |
| | 12.5mm deflection | 6.25mm deflection | 12.5mm deflection | 6.25mm deflection |
| PA1 | 1.78 | 3.03 | 0.42 | 1.44 |
| PA2 | 2.02 | 3.26 | 0.86 | 2.26 |
| PA3 | 2.10 | 3.93 | 0.60 | 2.21 |
| PB1 | 1.13 | 2.33 | 0.62 | 1.58 |
| PB2 | 1.85 | 3.02 | 0.47 | 1.25 |
| PC1 | 1.11 | 2.19 | 0.67 | 1.61 |
| PC2 | 1.19 | 2.93 | N/A | N/A |

The pile head rotation angle was recorded during the test and the results are shown in Figure 14. All piles exhibited almost the same behavior, which characterized by three distinct regions. In the first region, the rotation angle increased with loading as the pile rotated as a rigid body and the performance is mainly governed by the soil stiffness. In the second region, the rotation remained almost constant as the applied load increased. This behavior is attributed to the contribution of the passive resistance over the helical plate, which was mobilized due to the relatively large deformations and provided “fixation” at the location of the helix. As the load continued to increase, the pile itself started to deflect and additional rotation occurred in the third region.

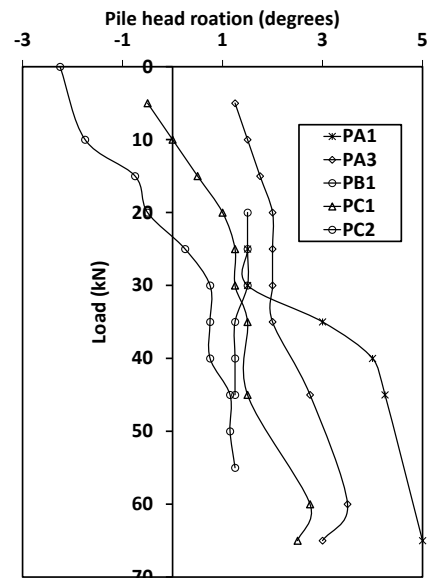


Figure 14: Variation of the pile head rotation with loading

5 CONCLUSIONS

The lateral performance of a novel ductile cast iron tapered helical pile was investigated in this study. 7 piles were installed in silty sand soil and were subjected to static and cyclic lateral load tests. The test piles included 5 tapered helical piles with 2 different average diameters and same taper angle and 2 straight-shaft helical piles. The effect of cyclic lateral loading on the pile lateral

capacity was also studied. The main conclusions drawn from this study are as follows:

1. The tapered piles generally exhibited stiffer response and higher ultimate capacity compared to the straight-shaft piles owing to the greater diameter and flexural rigidity at the top portion of the pile;
2. The results demonstrated that the spun cast iron with rough surface is a viable material for piling products.
3. The helical plate was found to significantly increase the lateral pile capacity for short piles.
4. The cyclic loading was found to significantly reduce the lateral stiffness and capacity of all tested piles. This was mainly attributed to the development of a gap along the upper portion of the pile and a zone of loose soil of the caved-in sand.

6 ACKNOWLEDGEMENTS

The authors would like to thank EBS Geostructural for funding the experimental program, Seamless Pole Inc. for manufacturing and providing the tested piles and Hassco Steel for providing the test site and logistic support.

7 REFERENCES

- AASHTO 2002. Standard Specifications for Highway Bridges, HB-17., American Association of State and Highway Transportation Officials.
- Allotey, N. and El Naggar, M. 2008. A numerical study into lateral cyclic nonlinear soil-pile response. *Canadian Geotechnical Journal*, 45(9): 1268-1281.
- ASTM C136 2014. Standard test method for sieve analysis of fine and coarse aggregates, ASTM international.
- ASTM D1556 2007. Standard Test Method for Density and Unit Weight of Soil in Place by the Sand-Cone Method, ASTM international.
- ASTM D2487 2011. Standard Practice for Classification of Soils for Engineering Purposes (Unified Soil Classification System), ASTM international.
- ASTM D3080 2011. Standard Test Method for Direct Shear Test of Soils Under Consolidated Drained Conditions, ASTM international.
- ASTM D4318 2010. Standard Test Methods for Liquid Limit, Plastic Limit, and Plasticity Index of Soils, ASTM international.
- Bagheri, F. and El Naggar, M. 2013. Effects of the installation disturbance on the behavior of the multi-helix screw anchors in sands, Montreal, Canada
- Bowles, J. 1996. Foundation analysis and design, 5th ed., McGraw hill.
- El Naggar, M. H. and Wei, J. Q. 1999. Response of tapered piles subjected to lateral loading. *Canadian Geotechnical Journal*, 36(1): 52-71.
- EIKasabgy, M. 2011. Dynamic and static performance of large-capacity helical piles in cohesive soils. *PhD thesis*. London, Canada: The University of Western Ontario.
- Fleming, K., Weltman, A., Randolph, M. and Elson, K. 2009. Piling engineering. 3rd ed., Taylor and Francis Group.
- Kulhawy, F. H. and Mayne, P. W. 1990. Manual on estimating soil properties for foundation design, Ithaca, New York: Cornell University
- Liao, S. S. C. and Whitman, R. V. 1986. Overburden correction factors for SPT in sand. *Journal of Geotechnical engineering Division*, 112(GT3): 373-377.
- Mayne, P. W. 1992. In-situ characterization of Piedmont residuum in eastern US. Belo Horizonte, National Science Foundation/USA: 89-93.
- Mayne, P. W. 2006. In-situ test calibrations for evaluating soil parameters: Overview Paper on In-Situ Testing-Singapore Workshop.
- Mayne, P. W., Christopher, B. and DeJong, J. 2002. Manual on subsurface investigations- Geotechnical site characterization, Washington, DC, Federal highway administration, U.S. Department of Transportation.
- Mayne, P. W. and Kulhawy, F. 1982. Ko-OCR Relationships in Soil. *Journal of the Geotechnical Engineering Division*, 108(6): 851-872.
- Pender, M. J. and Pranjoto, S. 1996. Gapping effects during cyclic lateral loading of piles in clay. Eleventh World Conference on Earthquake Engineering, Acapulco, Mexico, 23-28
- Poulos, H. G. and Davis, E. H. 1980. *Pile foundation analysis and design*, John Wiley and Sons Inc.
- Prakash, S. and Sharma, H. 1990. *Pile foundation in engineering practice*, John Wiley and Sons, New York. USA.
- Prasad, Y. and Rao, S. 1996. Lateral capacity of helical piles in clay. *Journal of Geotechnical Engineering*, 122(11): 938-941.
- Puri, V.K., Stephenson, R.W., and Goen, L. 1984. Helical anchor piles under lateral loading. In laterally loaded deep foundations: Analysis and performance. ASTM STP 835. Edited by J.A. Langer, E.T. Mosley, and C.D. Thompson. American Society for Testing and Materials: 194-213
- Sakr, M., El Naggar, M. H. and Nehdi, M. 2005. Lateral behaviour of composite tapered piles in dense sand. Proceedings of The Institution of Civil engineers- Geotechnical Engineering, 158(3): 145-157.
- Seamless-Pole-Inc. 2010. *Seamless pole*. [Online] Available at: <http://www.seamlesspole.com/>
- Skempton, A. W. 1986. Standard penetration test procedures and the effects in sands of overburden pressure, relative density, particle size, aging, and over-consolidation, *Geotechnique*, 36(3): 425-447.